THE DISCOVERY OF NEW IMPACT MELTS USING MINI-RF ON LRO. J. H. Madden[1], C. D. Neish[2], L. M. Carter[3], B. R. Hawke[4], and T. A. Giguere[4]. [1]Franklin and Marshall College, Lancaster, PA 17603, [2]Florida Institute of Technology, Melbourne, FL 32901, [3]NASA Goddard Space Flight Center, Greenbelt, MD 20770, [4]The University of Hawai'i at Manoa, Honolulu, HI 96822.

Introduction: The emplacement of lunar impact melt flows is not fully understood, partially due to a lack of statistics on which craters have melt deposits. Using data collected by the instruments onboard the Lunar Reconnaissance Orbiter (LRO), we surveyed the moon for new impact melts. Impact melts tend to be rough at radar wavelengths, so they stand out in maps of the circular polarization ratio (CPR) and total radar backscatter acquired using LRO's Mini-RF (MRF) instrument [1][2]. Since radars are capable of penetrating into the regolith by up to a few meters, we are able to locate melts that are buried and therefore have been unobserved in optical surveys [3]. Coupled with optical data from the LRO Camera (LROC) we are able to visually confirm the melts initially found using radar.

Mini-RF S-Band (12.6 cm) data cover 66% of the lunar surface and we have discovered many new melts using this method, increasing the number of known melts by over 20%. We were also able to revisit previously discovered melts and gather more accurate data on them. With the new melts we have discovered and with the updated data on known melts, we have significantly improved the current global statistics on lunar impact melts [4][5]. This new data sheds light on how these melt flows are emplaced during the impact process.

Method: Impact melts tend to have high radar backscatter and CPR, which are the result of wavelength-scale surface roughness. With LRO's MRF instrument we can map the CPR and backscatter of the lunar surface at S-Band (12.6 cm). These radar-bright features stand out in such a map, making it easy to identify them. Once a possible melt is found with MRF, we then confirm the melt with LROC data. (See Figure 1 for a comparison of MRF and LROC data.) After a melt is confirmed with optical imagery we then use data from LRO's Laser Altimeter (LOLA) to map the topography of the crater and Clementine UVVIS imagery to infer the downrange direction. From this data we record the crater location, diameter, melt length and direction, the direction of the lowest rim crest, and (where possible) direction downrange of the impact.

Results: Through our survey of the moon we identified 24 new impact melt flows (presented in Table 1). We describe a few particularly interesting examples in the sections below.

NE of Compton. This 5 km diameter crater is located 180 km to the NE of the crater Compton. It has one of the longest known melt flows relative to crater size. The melt extends 5.2 crater radii south-east from the crater. The melt follows topographic contours and is spread over multiple craters (Figure 1), suggesting that some melt overcame the topographic highs by a combination of ballisitic emplacement and sufficient flow velocity.

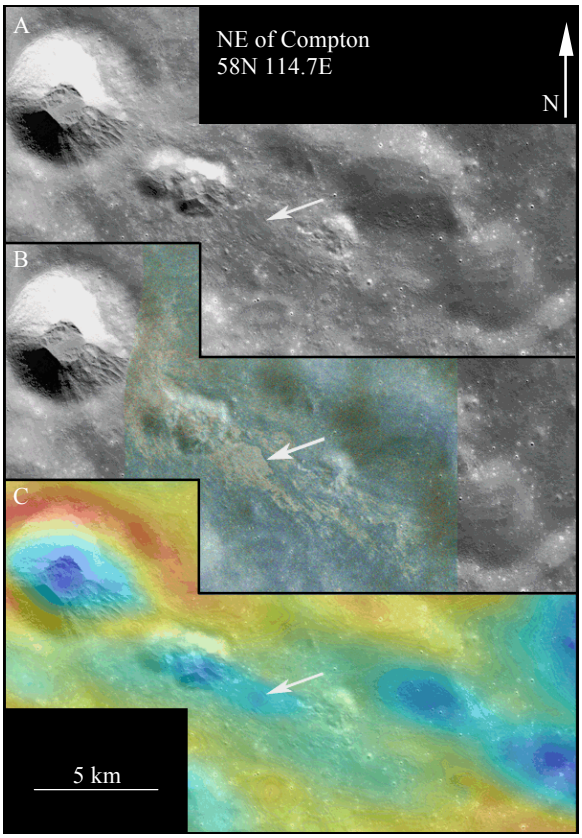

Figure 1: Multiple images showing the melt flow from the crater NE of Compton, indicated by a white arrow. (A) LROC images (M185155928R, M185148771L). (B) The same image with MRF data overlayed. The melt appears radar bright with higher CPR. (C) The LROC image with LOLA topography data overlayed. Notice how the melt flows from the point of lowest rim crest and continues downhill, ponding in local depressions.

Hayn. The Hayn melt flow is an example of how data from MRF is helping to reveal new lunar impact melts. Not immediately visible in optical data, the melt from Hayn can be seen clearly in the MRF data

(Figure 2). Hayn is a Copernican crater [6] with a diameter of 87 km. The melt can be seen stretching about 50 km to the south-east in the MRF data. Hayn is the second largest crater we found with melt in this survey and the melt flow direction corresponds to topographically lowest point in the rim crest.

Conclusions: With the data from LRO we were able to identify many new impact melt flows. The discovery of new examples of melt will allow for more in-depth studies of impact melts by providing a greater sample size. Along with an update in global statistics [4] this new survey will significantly change our understanding of how impact melts are emplaced.

References: [1] Carter L. M. et al. (2012) *JGR*. 117: E00H09, 1-13. [2] Campbell B. A. et al. (2010) *Icarus*, 208, 265. [3] Hawke B. R. and Head J. W. (1977) In: *Impact and Explosion Cratering,* Pergamon Press, New York, NY, pp. 815. [4] Neish C. D. et al. (2014), *LPSC XLV*. [5] Neish C. D. et al. (2014), submitted to *Icarus*. [6] Shirley, K.A. et al. (2012), *LPSC XLIII*.

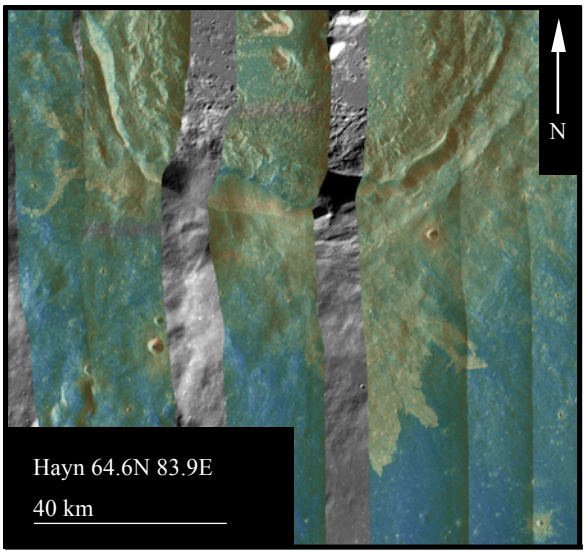

Figure 2. Hayn's melt flows are clearly visible in the MRF data, and confirmed in the optical data upon closer inspection. Here colorized CPR data is overlaid on total radar backscatter (purple represents a CPR of 0 and red represents a CPR of 1.2.)

Table 1: Displayed here are the 24 new impact melts discovered by this survey. In many cases it was difficult to determine the downrange direction, so these data points are left blank.

Crater	Diameter (km)	Lat. (°)	Long. (°)	Melt Length (Crater Radii)	Melt Direction	Downrange Direction	Lowest rim point direction
Vavilov	98	-0.9	138.8	0.69	ENE	-	ENE
Hayn	87	64.6	83.9	1.18	SE	-	SE
Helmholtz D	46	-66.1	54.1	0.26	SE	-	E
Newcomb	40	29.8	43.7	1	N	-	S
Thales	31	61.6	50.2	0.84	NE	-	SE
Slipher S	24	48.9	158.7	2	NE	-	NE
Larmor Q	22	28.7	176.3	0.86	S	-	S
Ventris M	16.2	-5.7	157.9	1.6	N	-	N
Janssen K	16	-46.2	42.3	1.65	W	-	W
Bessel	15.6	21.7	17.9	1.33	ENE	-	ENE
Gauss J	14	40.6	72.7	1	SE	-	SE
Pythagoras K	12	67.3	-75.8	0.25	NE	-	SE
Lagrange D	11	-34.9	-72.5	1.45	NE	-	NE
Rim of Virtanen	11	15.8	177.3	1.09	W	-	W
Inside Pingre	7	-58.9	-72.7	0.43	S	-	W
Eimmart A	7	24.1	65.7	1	N	-	SE
S of Tsinger	6.3	55.3	174.5	0.86	W	-	SW
NE of Compton	5.8	58	114.7	5.2	SE	E	SE
N of Tsinger	3.8	57.3	175.7	1.06	NW	-	NW
Herigonius K	3	-12.8	-36.5	1.67	NE	NE	SW
E of Polybius R	2.9	-25.7	27.9	3.34	S	NNW	SE
SE of Coriolis G	2.5	-0.4	175	0.9	SW	-	E
SE of Langevin	2.2	42.4	163.9	0.73	SE	-	NE, W, SE
SE of Olcott	1.5	17.4	120	1.33	SW	E	S